Journal of Applied Sciences

ISSN 1812-5654

science alert

ANSInet
an open access publisher
http://ansinet.com

Journal of Applied Sciences 7 (6): 820-825, 2007
ISSN 1812-5654

Classification of Heart Abnormalities Using Artificial Neural Network

Mohd Hanif Md Saad, Mohd Jailani Mohd Nor, Fadzlul Rahimi Ahmad Bustami and Ruzelita Ngadiran
MEMS in Automotives Application Research Group,
Department of Mechanical and Materials Engineering,
Universiti Kebangsaan Malaysia, 43600 Bandar Baru Bangi, Selangor, Malaysia

Abstract: This paper describes heart abnormalities classification procedures utilising features obtained from Time-Frequency Spectogram and Image Processing Techniques. Enhanced spatial features of time-frequency spectrogram were extracted and fed into a Multi-Layer, Back-Propagation trained Artificial Neural Network and the corresponding abnormalities were classified. A confidence factor is calculated for every classification result indicating the degree of belief that the classification is true. It was observed that the classification method was able to give 100% correct classification based on features that was extracted from the training data sets and the validation data sets.

Key words: Heart abnormalities classification, artificial neural network, simultaneous time-frequency analysis

INTRODUCTION

The objective of this research is to study and classify Human Heart Abnormalities using information obtained from Time-Frequency Spectrogram and Image Processing Technique through the application of Artificial Neural Network.

It is widely accepted that by measuring and observing the time domain electrocardiogram (ECG) of a human heart, a qualified medical practitioner would be able to determine the condition of the heart (whether the heart is normal or abnormal). The same process can be automated using a PC based system, for example, and given the same ECG, the program would be able to conclude the condition of the human heart.

The automated classification procedure has some advantages. Firstly, as it is implemented as a computer program, it can be exactly duplicated on other computers. This enable the same expertise to be widely available to a broader number of patient. Secondly, a computer program does not deteriorates with time, as compared to the human capability. Thus the automated system stays the same whilst the human doctor might become less and less comptenet as his age increases.

The ECG of a normal heart rate consists of the P wave, QRS complex and T wave and repeats as shown in Fig. 1.

Time and frequency domain features: However, time-domain ECG plots lack the signal intensity display of the frequency domain components. This is a great loss as frequency domain components contribute significantly in determining unique features of most engineering and scientific signals (Dripps, 1997).

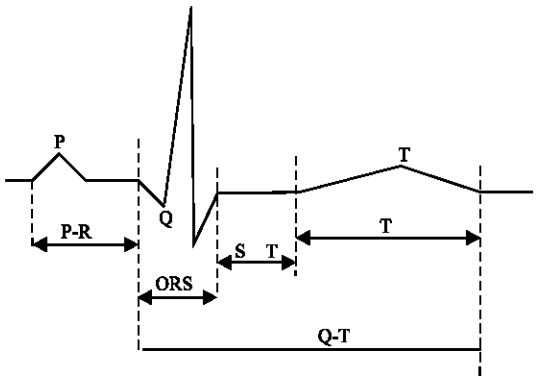

Fig. 1: PQRST complex of an ECG pulse (Enderle *et al.*, 2000)

The frequency analysis of such signals via Fourier techniques is fundamentally unsatisfactory since they are based upon modeling the signal as a linear combination of sinusoids extending throughout the duration of the signal. The Fourier analysis is good at determining what frequencies are present (i.e., it provides good frequency discrimination), but poor at pinpointing when these frequencies occur (i.e., it has poor time localization) (Crowe, 1997; Hlawatsch *et al.*, 1992; Haghighi-Mood and Torry, 1997).

Corresponding Author: Mohd Hanif Md Saad, MEMS in Automotives Application Research Group, Department of Mechanical and Materials Engineering, Universiti Kebangsaan Malaysia, 43600 Bandar Baru Bangi, Selangor, Malaysia Tel: +60-3-89216678 Fax: +60-3-89216145

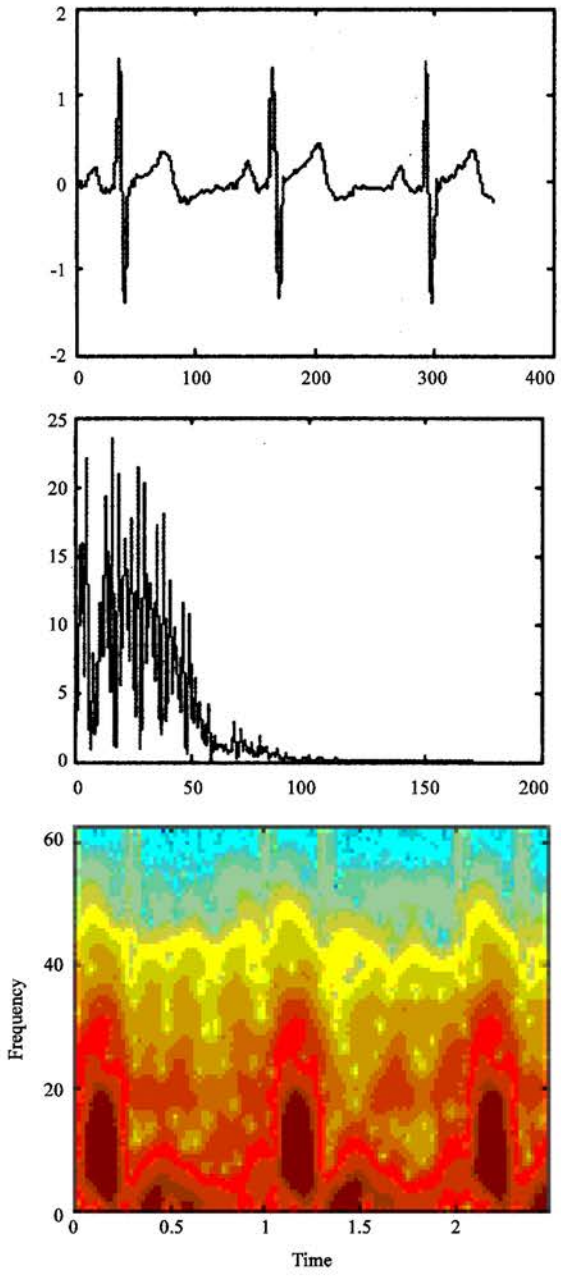

Fig. 2: ECG Plots in Time Domain (Top), Frequency Domain (Middle), Time-Frequency Domain (Bottom)

Popular simultaneous time-frequency analysis techniques include the Wavelet Transform (Ikeda *et al*., 1997) and the Short Time Fourier Transform. Time domain, frequency domain and simultaneous time-frequency domain display of ECG signals is shown in Fig. 2.

Short time fourier transform (STFT): The short-time Fourier transform (STFT) is a linear time-frequency representation (TFR) used to present changes in the signal that vary with time. The Fourier transform does not explicitly show the time location of the frequency components, but some form of time location can be obtained by using a suitable pre-windowing (Hlawatsch and Boudreaux-Bartels, 1992). The STFT approach is to perform a Fourier Transform on only a small section (window) of data at a time, thus mapping the signal into a two-dimensional (2-D) function of time and frequency. The transform is described mathematically as:

$$X(\omega,a) = \int_{-\infty}^{\infty} x(t)g(t-a)e^{-j\omega t}dt \quad (1)$$

where, g (t) may be defined as a simple box or pulse function.

In this study, the Blackman window with a window size of 256 (50% overlapping) discrete data out of a total of 512 discrete data was used. The Blackmann method of windowing was choosen because it gives minimum variation on spectrum shape and colour compared to other techniques. The discrete version of the Blackman window can be described by the equation below:

$$w[k+1] = 0.42 - 0.5\cos\left(2\pi\frac{k}{n-1}\right) + 0.08\cos\left(4\pi\frac{k}{n-1}\right), \quad (2)$$
$$k = 0,\ldots,n-1$$

Selection of frequency band: The useful frequency band for the ECG signal to be studied was decided to be between 0.5 Hertz (Hz) to 59 Hz. Detailed signal analysis by prior researchers indicates that the P-wave and T-wave mainly contain frequency components that are far below 60 Hz. The R-wave also mainly contains frequency components that are below 60 Hz but it also contains some frequency components that are beyond 60 Hz. Through the use of a band pass filter, the signal bandwidth was selected to be between 0.5 to 59 Hz. Such a filter will effectively reduce 60 Hz noise (normally acquired through powerline), have little effects on P-wave and T-wave and finally produce some acceptable distortion on the R-wave. Cut-off frequency above 0.5 Hz was chosen to avoid the low-frequency noise due to respiration and electrode movement that below accous 0.03 Hz.

Linear spatial domain filter: One of the simplest linear, spatial image processing techniques used in machine vision is the convolution operation. The operation can be described as follows:

For any given planar image P and a 3×3 elements mask G described by both (3) and (4) below,

$$P = \begin{bmatrix} \cdot & \cdot & \cdot & \cdot & \cdot & \cdot & \cdot & \cdot \\ \cdot & \cdot & \cdot & \cdot & \cdot & \cdot & \cdot & \cdot \\ \cdot & \cdot & p_{x_{n-1}y_{n-1}} & p_{x_ny_{n-1}} & p_{x_{n+1}y_{n-1}} & p_{x_{n+2}y_{n-1}} & \cdot & \cdot \\ \cdot & \cdot & p_{x_{n-1}y_n} & p_{x_ny_n} & p_{x_{n+1}y_n} & p_{x_{n+2}y_n} & \cdot & \cdot \\ \cdot & \cdot & p_{x_{n-1}y_{n+1}} & p_{x_ny_{n+1}} & p_{x_{n+1}y_{n+1}} & p_{x_{n+2}y_{n+1}} & \cdot & \cdot \\ \cdot & \cdot & p_{x_{n-1}y_{n+2}} & p_{x_ny_{n+2}} & p_{x_{n+1}y_{n+2}} & p_{x_{n+2}y_{n+2}} & \cdot & \cdot \\ \cdot & \cdot & p_{x_{n-1}y_{n+3}} & p_{x_ny_{n+3}} & p_{x_{n+1}y_{n+3}} & p_{x_{n+2}y_{n+3}} & \cdot & \cdot \\ \cdot & \cdot & \cdot & \cdot & \cdot & \cdot & \cdot & \cdot \end{bmatrix} \quad (3)$$

$$G = \begin{bmatrix} g_{11} & g_{12} & g_{13} \\ g_{21} & g_{22} & g_{23} \\ g_{31} & g_{32} & g_{33} \end{bmatrix} \quad (4)$$

the convoluted image P* is given as:

$$P^*(x,y) = \sum_{i=0}^{(m-1)} \sum_{j=0}^{(n-1)} G(i,j)P(x+i-1, y+j-1) \quad (5)$$

Different coefficient value will give different filter behavior (Gonzales and Woods, 2002).

Gaussian filter: The Gaussian filter smoothes a given image P. It is made from the same structure in (3), (4) and (5) with specialized value of filter coefficient. The values varies according to requirement and specification. One such set of values is shown in Eq. 6 below:

$$G = \begin{bmatrix} 0.011 & 0.084 & 0.011 \\ 0.084 & 0.619 & 0.084 \\ 0.011 & 0.084 & 0.011 \end{bmatrix} \quad (6)$$

Sobel edge detection: In Sobel Edge detection, two operators were used, G_x and G_y to calculate approximations of the derivatives, one for horizontal changes and one for vertical. The Sobel operators calculates the gradient of the image intensity at each point, giving the direction of the largest possible increase from light to dark and the rate of change in that direction. The result therefore shows how abruptly or smoothly the image changes at that point and therefore how likely it ist that part of the image represents an edge, as well as how that edge is likely to be oriented.

The operators follow the same structure as (5). If P is defined as the source image and G_x and G_y are the two operators described above, the latter are computed as:

$$\begin{bmatrix} \Delta P_x \\ \Delta P_y \end{bmatrix} = \begin{bmatrix} G_x * P \\ G_y * P \end{bmatrix} \quad (7)$$

where

$$G_x = \begin{bmatrix} -1 & 0 & +1 \\ -2 & 0 & +2 \\ -1 & 0 & +1 \end{bmatrix}; G_y = \begin{bmatrix} +1 & +2 & +1 \\ 0 & 0 & 0 \\ -1 & -2 & -1 \end{bmatrix} \quad (8)$$

At each point in the image, the resulting gradient approximations can be combined to give the gradient magnitude, using:

$$\Delta P = \sqrt{\Delta P_x^2 + \Delta P_y^2} \quad (9)$$

Using this information, the gradient's direction is calculated as below:

$$\Theta = \arctan\left(\frac{\Delta P_y}{\Delta P_x}\right) \quad (10)$$

where, for example, Θ is 0 for a vertical edge which is darker on the left side.

Non-linear spatial domain filter: median filter: A median filter is a non-linear filter. In a median filter, the median value for the pixels in the processed window is used to replace the current pixel under processed. For example, consider a pixel (with the absolute value of 150) that is surrounded by 8 other pixels shown in equation (11) below. Each pixels value is then arranged incrementally and the original pixel value in the middle is then replaced with a new value which is the value median of the arranged pixels (Gonzales and Woods, 2002; Fisher *et al.*, 1994). Equation (11) describes how median filter is implemented.

$$P = \begin{bmatrix} \cdot & \cdot & \cdot & \cdot & \cdot & \cdot & \cdot & \cdot \\ \cdot & \cdot & \cdot & \cdot & \cdot & \cdot & \cdot & \cdot \\ \cdot & \cdot & 124 & 126 & 127 & \cdot & \cdot & \cdot \\ \cdot & \cdot & 120 & 150 & 125 & \cdot & \cdot & \cdot \\ \cdot & \cdot & 115 & 119 & 123 & \cdot & \cdot & \cdot \\ \cdot & \cdot & \cdot & \cdot & \cdot & \cdot & \cdot & \cdot \\ \cdot & \cdot & \cdot & \cdot & \cdot & \cdot & \cdot & \cdot \\ \cdot & \cdot & \cdot & \cdot & \cdot & \cdot & \cdot & \cdot \end{bmatrix} \quad (11)$$

Original Value : 150
Neighborhood values : 15,119,120,123,124,125,126,127,150
Median Value : 124

Pulse counting from binary image: The spectrogram obtained from the STFT operation is converted into a grayscale image and binary thresholded to produce a black and white only representation of the original STFT spectrogram.

At a selected frequency ($f_{selected}$ = 45 Hz), the number of transitions made by pixel value are calculated. For example, if a line of pixel at any height is extracted, the following representation might be obtained:

$$000111111110000001111110 \quad (12)$$

From the example above, 4 transitions (N_T) can be obtained. The pixels located in a pulse area are indicated by 1. Since the transition included from 0 to 1 and 1 to 0, the number of total pulse is actually $N_P = N_T/2$. In the above example, there are actually 4/2 = 2 pulses detected. This method is by far not the most robust and precise pulse counting method, but it was observed throughout the study that the results it produced was acceptable.

Euler number: Euler Number is defined as the number of connected components. It is a topological property that is useful for region description. The number of holes H and connected components, C in an image can be used to define the Euler Number, E:

$$E = C-H \quad (13)$$

The regions shown in Fig. 3, for example, have Euler numbers equal to 0 and -1, respectively, because the left figure has one connected component and one hole and the right component has one connected component but two holes (Gonzales and Woods, 2002).

Types of heart abnormalities investigated: The types of heart abnormalities which were studied in this research are described in Table 1. The data were obtained online from www.physionet.org (Goldberger *et al.*, 2000).

Features observed: The features from the processed spectrogram image which was extracted and used for classification is described in Table 2.

Identification method: A multi-layered perceptron, back-propagation trained Artificial Neural Network (ANN) was used to identify the different types of heart abnormalities.

Generally, ANN consist of a number of simple and highly interconnected processor called neuron. The

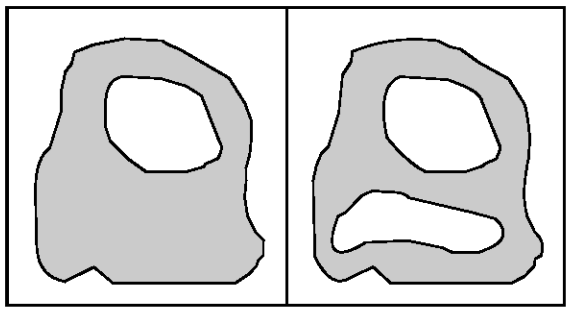

Fig. 3: Regions with Euler number equal to 0(Left) and -1 (Right)

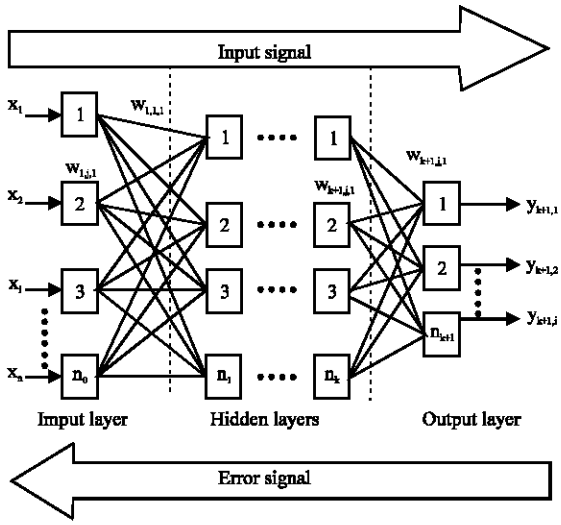

Fig. 4: Feed Forward, Back Propagation Trained Neural Network

neurons are connected by weighted links that pass signals from one neuron to another (Negnevitsky, 2002).

Multilayer neural network are Feed Forward neural network with one or more hidden layer (Fig. 4). A network consist of input layer, hidden layers and output layer. Network are adjusted or trained so that a particular input leads to specific target output. Hidden layers are important to extract useful information from inputs and use them to predict output.

A network with input vector, X is transmitted through a connection that is multiplied by weight $W_{1,j,i}$ and passes through an activation function $f_1(...)$ to give the output $y_{1,i}$.

The output is then is fed into another activation function $f_{k+1}(..)$ to produce the output for node-I at layer (k+1), $y_{k+1,i}$. The process is repeated towards the end of the layers. The process is best described by the equation below:

Table 1: Type of heart abnormalities and their description

Abnormality	Description
Normal	Normal working heart
Atrial fibrillation	Atrial Fibrillation is an abnormality of the heart in which the atrial of heart is not depolarized completely(activated). The P peak of the time domain ECG is not very clear, but in time-frequency domain, the pulses are narrower compared to the pulses from the normal heart.
Supraventricular arrhythmia	Hearts with Supraventricular Arrhythmia produces the maximum peak frequency below 50 Hertz.
Ventricular tachyarrhythmia	In this kind of abnormality, the number of pulses in every period is considerably bigger as compared to other kind of abnormalities and normal heart
Myocardial infarction	This kind of abnormality genera`tes pulses which are not firm compared to the normal pulse due to the weakness of the heart to execute normal heart activity.

Table 2: Features observed

Features	Description
W_P	The width of individual pulses in the spectrogram
H_P	The height of individual pulses in the spectrogram
N_P	The number of pulses recorded in 3.125 second in the spectrogram
I_P	The intensity of each pulses in the spectrogram
NE_P	The Euler Number calculated on individual pulse in the spectrogram
NE_{IMG}	The Euler Number calculated on the overall image of the spectrogram
$NE_{P,SED}$	The Euler Number calculated on the image of containing edges of a single pulse
$NE_{IMG,SED}$	The Euler Number calculated for the edges of the overall image of the spectrogram

Table 3: Overall classification test results

Data	No. of data used in training	No. of data used in validation	% Correct classification
Original data	30	15	100
Interpolated data	60	15	100
Total	90	30	100

Table 4: Sample classification test results

Abnormality	Height (j = 1)	Pulse (j = 2)	Width	Int.	Euler ori	Euler sobel	Euler All	Euler sobel All	CF	√ / ×
Normal	1.000	0.500	0.875	0.750	0.625	0.625	0.625	0.625	1.000	√
Atrial fibrillation	1.000	0.100	0.500	0.875	0.750	0.875	1.000	0.750	1.000	√
Myocardial infarction	0.675	1.000	0.625	0.125	0.500	0.500	0.375	0.250	0.960	√
Supraventricular arrhythmia	1.000	0.500	1.000	1.000	0.125	0.875	1.000	0.875	1.000	√
Ventricular tachyarrhythmia	0.250	1.000	0.125	1.000	0.750	0.250	1.000	0.625	0.910	√
Normal	1.000	0.500	0.875	0.750	0.625	0.625	0.250	0.625	1.000	√
Atrial fibrillation	1.000	0.100	0.500	0.125	0.750	0.875	1.000	0.750	1.000	√
Myocardial infarction	0.250	1.000	0.250	0.500	0.500	0.500	0.625	0.250	0.906	√
Supraventricular arrhythmia	1.000	0.500	1.000	1.000	0.125	0.875	1.000	0.875	1.000	√
Ventricular tachyarrhythmia	0.250	1.000	0.875	0.000	0.000	0.250	1.000	0.625	0.906	√

$$y_{k+1,i} = f_{k+1}\left[\sum_{j=1}^{n_k} W_{k+1,j,i} \times f_k\left(\sum_{j=1}^{n_{k-1}} W_{k,j,i} y_{k,i} + b_{k,i}\right) + b_{k+1,i}\right] \quad (14)$$

where:

$y_{k+1,i}$: Output at node-I of layer-(k+1)
f_{k+1} : Activation function at layer-(k+1)
$W_{k+1,j,i}$: Weight of the connection between node-I of layer-(k+1) and node-j of layer-k
$b_{k+1,i}$: Bias at node-I of layer-(k+1)
n_k : Number of nodes from layer-k which is Connected to node-I of layer-(k+1)

The weight are adjusted to reduce error between actual and desired output pattern during training. This error is minimized until it reach at certain objective value.

In this study a 3 layer, back-propagation trained ANN was used to identify the abnormality. The input layers have 9 nodes comprising the features (Table 2) that were extracted from the heart beat. The output layer has 6 nodes denoting the different types of abnormalities (Table 1). Each nodes gives the certainity factor (cf) of the classification process. A cf of closest to or equal to one represents the node with the highest probability of identifying the correct abnormality. Thirty original data and sixty interpolated data were used for training the ANN. Fifteen original data and fifteen interpolated data were used to validate the ANN.

RESULTS

The overall classification result is shown in Table 3. Table 4 shows 10 numerical example of the classification results.

The first five rows shows the cf of the classified abnormality for the data set which were used in training the ANN. The last five rows shows the cf of the classified abnormality for the dataset which was not used in the training process. In both sets of data, the system was able to correctly classify the investigated abnormalities with

100% accuracy. The cf for the classified abnormality varies but the values were either close to or equal to 1.00, which indicates strong belief in the result.

DISCUSSION AND CONCLUSION

The detection results obtained showed that the system functions very well and gives very good detection result (100% accuracy). It is therefore concluded that the objective of this research has been achieved. Future enhancement in this research includes the inclusion of more data in the knowledge base and cf extraction. Further testing involving significantly larger test set is also planned in the near future to further test the robustness and accuracy of this system.

ACKNOWLEDGMENT

This research was supported by the Ministry of Science, Technology and Environment, Malaysia under the 8th Malaysia Plan's IRPA 03-02-02-0016-SR0003/07-02 Grant.

REFERENCES

Crowe, J.A., 1997. The wavelet transform and its application to biomedical signals. Time-Frequency Analysis of Biomedical Signals (Digest No. 1997/006), IEE Colloquium on Year: 29 Jan 1997: 2/1-2/3.

Dripps, J.H., 1997. An introduction to time frequency methods applied to biomedical signals. Time-Frequency Analysis of Biomedical Signals (Digest No. 1997/006), IEE Colloquium on Year : 29 Jan 1997.

Enderle, J., S. Slanchard and J. Bronzio, 2000. Introduction to Biomedical Engineering. San Diego. Academic Press.

Fisher, B., S. Perkins, A. Walker and E. Wolfart, 1994. Spatial Filters-median Filter. (Online) http://www.cee.hw.ac.uk/hipr/html/median.html (6 April 2006)

Goldberger, A.L., L.A.N. Amaral, L. Glass, J.M. Hausdorff, P.C. Ivanov, R.G. Mark, J.E. Mietus, G.B. Moody, C.K. Peng and H.E. Stanley, PhysioBank, PhysioToolkit and PhysioNet: Components of a New Research Resource for Complex Physiologic Signals. Circulation 101(23):e215-e220 [Circulation Electronic Pages; http://circ.ahajournals.org/cgi/content/full/101/23/e215]; 2000 (June 13).

Gonzales, R.C. and R.E. Woods, 2002. Digital image processing, 2nd Edn. New Jersey. Prentice-Hall, pp: 164, 234, 661-663.

Haghighi-Mood, A. and J.N. Torry, 1997. Time Frequency Analysis of Systolic Murmurs. Time-Frequency Analysis of Biomedical Signals (Digest No. 1997/006), IEE Colloquium on Year: 29 Jan 1997.

Hlawatsch, F. and G. Boudreaux-Bartels, 1992. Linear and quadratic time-frequency signal representations. IEEE Signal Process Mag, 9: 21-67.

Ikeda, K., B. Vaughn and S. Quint, 1997. Wavelet decomposition of heart period data. Proceeding of The First Joint BMES/EMBS Conference Serving Humanity, Advancing Technology, Oct. 13-16: 99.

Negnevitsky, M., 2002. Artificial intelligence, a guide to intelligent systems, Essex. Pearson Education Ltd., pp: 78.